Complex metallic alloys in the Ce–Au–Sn system: a study of the atomic and electronic structures

2008 J. Phys.: Condens. Matter 20 095218

(http://iopscience.iop.org/0953-8984/20/9/095218)

J. Phys.: Condens. Matter **20** (2008) 095218 (7pp) doi:10.1088/0953-8984/20/9/095218

Complex metallic alloys in the Ce–Au–Sn system: a study of the atomic and electronic structures

S Kenzari[1,2], V Demange[2,3], P Boulet[1,2,4], M C de Weerd[1,2], J Ledieu[1,2], J M Dubois[1,2] and V Fournée[1,2]

[1] Laboratoire de Science et Génie des Matériaux et de Métallurgie, UMR 7584 CNRS, Nancy-Université, Ecole des Mines de Nancy, Parc de Saurupt, 54042 Nancy, France
[2] Institut Jean Lamour, FR 2797 CNRS-INPL-UHP, Nancy-Université, Ecole des Mines de Nancy, Parc de Saurupt, 54042 Nancy, France
[3] Laboratoire de Science et Génie des Surfaces, UMR 7570 CNRS, Nancy-Université, Ecole des Mines de Nancy, Parc de Saurupt, 54042 Nancy, France

E-mail: pascal.boulet@mines.inpl-nancy.fr

Received 11 December 2007, in final form 24 January 2008
Published 14 February 2008
Online at stacks.iop.org/JPhysCM/20/095218

Abstract

We report the formation of a new stable quasicrystal approximant in the Ce–Au–Sn system. The crystalline structure of the $Ce_{15}Au_{65}Sn_{20}$ compound is investigated by x-ray diffraction and is found to be of similar structure type to the $Zn_{17}Sc_3$ 1/1 approximant. Large clusters with icosahedral symmetry are located at the node of the body-centred cubic (bcc) unit cell ($a = 1.5190$ nm) containing 161 atoms. We have used transmission electron microscopy to emphasize the relationship of this new compound with the icosahedral space group. The valence band has been investigated by photoemission spectroscopy and shows an indication of Van Hove singularities in the density of states, characteristic of quasicrystalline and related approximant phases. We expect similar 1/1 approximant and possibly icosahedral phases to be discovered in the new RE–Au–Sn systems (where RE is rare earth). We also found a hexagonal phase with a large unit cell possessing local icosahedral order, co-existing as a minority phase.

(Some figures in this article are in colour only in the electronic version)

1. Introduction

A new stable icosahedral quasicrystal has been found recently in the Zn–Mg–Sc system [1]. The atomic structure of this phase is locally similar to the cubic phase $Zn_{17}Sc_3$ ($Im\overline{3}$, $a = 1.3854$ nm), possessing the same cluster units [1, 2]. These clusters have icosahedral symmetry and consist of three concentric shells: an inner dodecahedron at 0.37 nm from the bcc nodes, decorated by Zn atoms, surrounded by an icosahedron of Sc atoms at 0.49 nm, and an outer icosidodecahedron of Zn atoms at 0.57 nm [1, 3]. In the cubic phase, the clusters are located at the node of the bcc unit cell and are glued together by Zn atoms, forming a distorted triacontahedron. The cubic phase is called a 1/1 approximant of the icosahedral phase because its lattice parameter a can be related to the six-dimensional lattice parameter a_{6D} of the icosahedral quasicrystal (by the formula $a = [(2/(2 + \tau))^{1/2}(p + q\tau)a_{6D}]$, where τ is the Golden mean and p and q are two successive Fibonacci numbers ($p/q = 1/1$ in this case)). Following the discovery of the i-$Zn_{81}Mg_4Sc_{15}$ phase, a number of icosahedral phases has been found by using chemical substitution, like i-$Cu_{48}Ga_{34}Mg_3Sc_{15}$, i-$Zn_{84}Mg_9Ti_7$, i-$Zn_{75}T_{10}Sc_{15}$ (T = Mn, Fe, Co, Ni) [4–6]. All these phases have a common number of valence electrons per atom, e/a, of ∼2.0 to 2.15, such that their Fermi sphere is tangential to a prominent pseudo-Brillouin zone, thus satisfying the Hume-Rothery stabilization criterion [5]. Band structure calculation performed for the $Zn_{17}Sc_3$ confirmed the existence of a minimum in the density of states at the Fermi level, as expected for Hume-Rothery alloys, but revealed that sp–d hybridization is a more important factor in the formation of this pseudo-gap than the Fermi surface–Brillouin zone interaction [7]. The

[4] Author to whom any correspondence should be addressed.

atomic structure and the stabilization mechanism of the Zn–Mg–Sc system are similar to those of Cd-based quasicrystals and approximants [7–9]. However, the cluster units are slightly different. Whereas the inner dodecahedron is empty in the $Zn_{17}Sc_3$ approximant, a Cd tetrahedron occupies its centre in the Cd–Yb 1/1 approximant [10, 11]. As in the Zn–Mg–Sc system, a number of icosahedral phases having similar structure to the i-Cd–Yb compound has been found by using appropriate chemical substitutions in Au–In–Yb, Ag–In–Yb, etc [12–16]. These chemical substitutions again preserve the valence electron concentration, with valence values equal to 1 for Au and Ag, 2 for Cd and 3 for In.

In this paper, we report the formation of a new, stable, complex metallic alloy in the Ce–Au–Sn system with a structure similar to the $Zn_{17}Sc_3$ 1/1 approximant. This system has already been studied by one of us, in a search for new heavy-fermion compounds expected in Ce-containing alloys [17]. Here, we have re-investigated the structure of the bcc $Ce_3Au_{14.2}Sn_{2.7}$ ($Ce_{15.1}Au_{71.4}Sn_{13.5}$) phase using transmission electron microscopy (TEM) to emphasize its relationship with the icosahedral space group. The valence band has been measured by photoemission spectroscopy and shows an indication of Van Hove singularities in the density of states, characteristic of quasicrystalline and related approximant phases. We also report the existence of another complex metallic phase in this system, exhibiting hexagonal symmetry and local icosahedral order.

2. Experimental methods

A polycrystalline ingot was obtained by arc-melting stoichiometric amounts of the constituent elements under an atmosphere of high-purity argon on a water-cooled copper hearth, using a Zr getter. Starting materials were used as supplied by commercial manufacturers in the form of 2N5 cerium blocks, 3N7 tin shot and 2N5 gold shot. Homogeneity of the sample was ensured by turning over and re-melting the button several times. Weight losses during the melting procedure were below 0.5%. According to [17], the homogeneity domain at 750 °C of the bcc phase extends from $Ce_3Au_{13}Sn_4$ ($Ce_{15}Au_{65}Sn_{20}$) to $CeAu_5Sn$ ($Ce_{14.3}Au_{71.4}Sn_{14.3}$), with a general formulae $Ce_3Au_{15\pm x}Sn_{3\pm y}$, $x \leqslant 2$ and $y \leqslant 1$. These compositions were determined by electron probe microanalysis. Here a sample was prepared with nominal composition $Ce_{15}Au_{65}Sn_{20}$, consistent with the composition determined by energy dispersive x-ray analysis ($Ce_{11}Au_{66}Sn_{23}$). According to [17] and the present study, the structure is stable upon annealing up to 750 °C.

The structure of this sample was checked from x-ray powder diffraction data collected on a D501 diffractometer (Bragg–Brentano geometry, $\lambda_{Co\ K\alpha 1} = 0.178\,89$ nm). Samples for TEM investigation were prepared by classical polishing followed by an ion milling step performed with the help of a Gatan PIPS device. Electron diffraction patterns (EDPs) were obtained by TEM in the selected area electron diffraction mode (SAED) with a 200 kV accelerating voltage (Philips CM200).

The valence spectra were acquired at room temperature using a He I (21.2 eV) lamp and a SPHERA analyser with a base pressure of 2×10^{-11} mbar. The energy resolution is estimated from the width (16%–84%) of the Fermi edge measured on a polycrystalline Ag sample (~100 meV), which corresponds approximately to the width of the Fermi function $4k_BT \sim 100$ meV. Measurements were performed on a polycrystalline sample (5×5 mm^2) presenting a flat surface prepared by mechanical polishing (diamond paste, 1 μm). The surface was cleaned in ultra-high vacuum by cycles of sputtering (Ar^+, 2 keV) and annealing up to 720 K, until no traces of contamination could be detected by x-ray photoelectron spectroscopy (XPS). The near-surface chemical composition calculated from Au 4f, Sn 3d and Ce 3d core levels was consistent with the bulk composition.

Table 1. Atomic parameters determined by x-ray powder diffraction for the $Ce_{15}Au_{65}Sn_{20}$ compound (SG: $Im\bar{3}$ no 204) $a = 1.5190(1)$ nm ($Rp = 16.0$, $Rwp = 15.1$, $R_B = 9.6$ and $R_f = 8.3$).

Atom	Site	x	y	z	Occ
Au(1)	24g	0.0	0.2433(6)	0.0914(5)	0.76(3)
Ce	24g	0.0	0.1905(5)	0.3055(5)	1
Au(2)	24g	0.0	0.4060(3)	0.3482(3)	1
Au(3)	48h	0.1069(2)	0.3446(2)	0.1989(2)	1
Sn(1)	12e	0.1854(7)	0.0	0.5	1
Au(4)	12d	0.4037(6)	0.0	0.0	1
Au(5)	16f	0.1511(4)	—	—	0.5
Sn(2)	16f	0.1511(4)	—	—	0.5
Sn(3)	16f	0.2654(2)	—	—	0.45(2)

3. Results

3.1. Structural model of $Ce_{15}Au_{65}Sn_{20}$

Figure 1 shows the full profile analysis of the x-ray powder diffraction pattern obtained using the Rietveld method via the Fullprof program [18] for a sample with nominal composition $Ce_{15}Au_{65}Sn_{20}$. The crystal structure has been refined in the centrosymmetric space group $Im\bar{3}$, as for $Zn_{17}Sc_3$ or Cd_6Yb. The refinement has been performed first in a profile matching mode, using 11 instrumental parameters and the unit cell parameter. Then, according to the crystal structure reported in [17], the atomic positions were added in the refinement, leading to 25 parameters and leading to the reliability factors $R_B = 0.105$ and $R_f = 0.095$. The final refinements were performed including the occupation factor of Au(1) and Sn(3), leading to $R_B = 0.096$ and $R_f = 0.083$. No departure from other crystallographic sites could be evidenced by further refinements. The result of the refinement, the lattice parameters and the standardized atomic positions are listed in table 1. The unit cell contains 161 atoms and the composition of the compound derived from the refinement is $Ce_3Au_{13.8}Sn_{3.4}$ ($Ce_{14.9}Au_{68.3}Sn_{16.8}$). The R factors are relatively high, compared to usual values achieved for simpler structures. This can be ascribed to the large number of atoms in the unit cell and the chemical disorder associated with specific sites. However, we found that the cluster description that is explained below is a robust feature.

As in the $Zn_{17}Sc_3$ 1/1 approximant, large atomic clusters with icosahedral symmetry are located at the node of the bcc

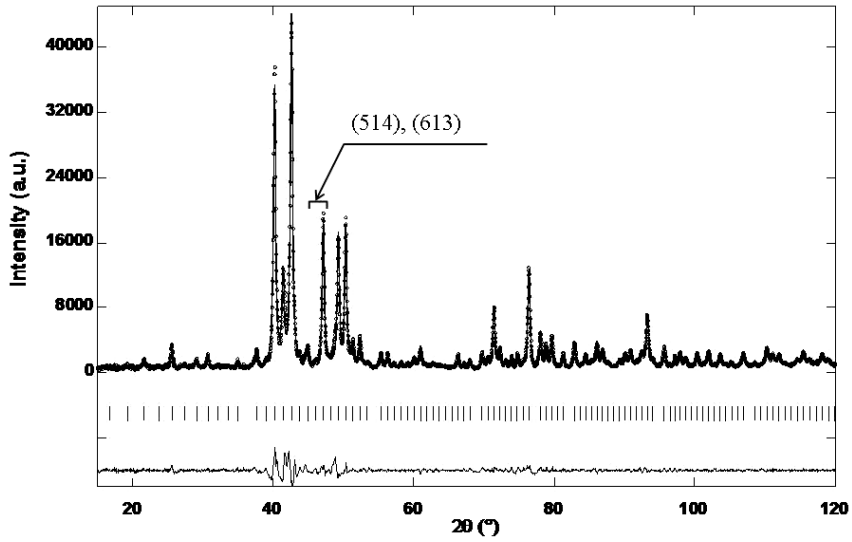

Figure 1. X-ray powder pattern of the alloy with nominal composition $Ce_{15}Au_{65}Sn_{20}$, showing an almost pure $Ce_3Au_{14.2}Sn_{2.7}$ structure type phase. The symbols represent the observed points; the solid lines represent the calculated profile and the difference between the observed and calculated profiles. The ticks correspond to $2\theta_{hkl}$ Bragg positions from the cubic $Im\bar{3}$ unit cell.

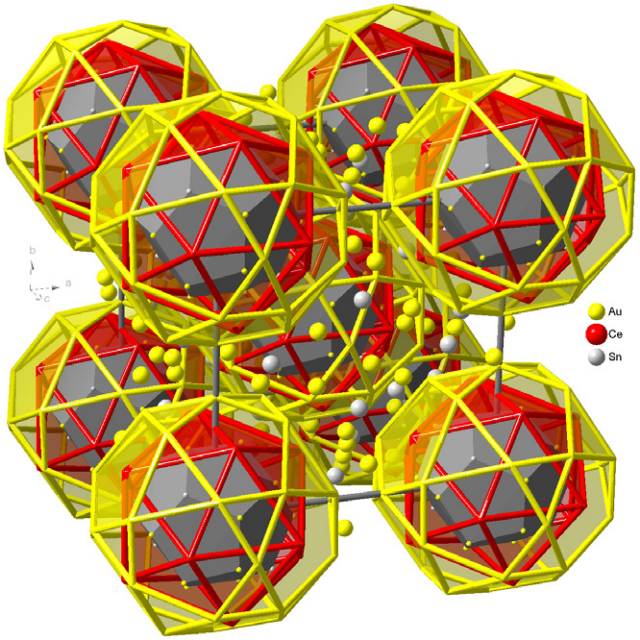

Figure 2. Representation of the atom cluster at the 000 and 1/2, 1/2, 1/2 positions in the bcc $Ce_{15}Au_{65}Sn_{20}$ lattice. The successive shells of the cluster can be recognized: inner $(Sn, Au)_{20}$-dodecahedron, the Ce_{12}-icosahedron (red) and the outer Au_{30}-icosidodecahedron.

unit cell, as shown in figure 2. Each cluster consists of three successive shells. The first shell is an empty dodecahedron decorated by 12 Au and eight Sn atoms at 0.39 nm from the bcc nodes. The second shell is a perfect icosahedron decorated by 12 Ce atoms at 0.54 nm. The third shell consists of an icosidodecahedron decorated by 30 Au atoms at 0.61 nm. The glue atoms, located in between the clusters, are either gold or tin atoms. In the centrosymmetric space group $Im\bar{3}$, it is not possible to differentiate between gold and tin atomic positions on the first dodecahedron. As explained in [17], the crystal structure can also be solved in the space group I23. This allows discrimination between gold and tin positions. We distinguish the two inner Sn_4-(grey) and Au_4-tetrahedra (yellow), corresponding to the Sn(2) and Au(5) atomic positions, respectively. Then, the two tetrahedra build a pseudo-cube, each faces of the cube then being bicapped by two Au(1) atoms, leading to the $(Sn, Au)_{20}$-dodecahedron. In summary, the structure of the $Ce_{15}Au_{65}Sn_{20}$ cubic phase is very similar to that of the $Zn_{17}Sc_3$ 1/1 approximant. Only the deficient Sn(3) site, corresponding to glue atoms, allows us to distinguish between both structures. In the following, we use TEM to investigate its relationship with the icosahedral space group.

3.2. Electron diffraction study

The orientation of an icosahedral cluster embedded in a cube can be defined by projecting the vectors connecting its centre to six of its vertices onto the cubic lattice. Directions corresponding to cluster vertices are expressed in the cubic basis with irrational coordinates which are powers of the golden mean τ ($\tau = 2\cos\pi/5$), a geometrical consequence of an icosahedra. In the case of the bcc phase studied here, the five-fold axes of the icosahedra are parallel to $\langle 1\tau 0\rangle$ directions, which are close to the $\langle 580\rangle$ directions. Figure 3(a) is an EDP taken along the [580] zone axis of the bcc $Ce_3Au_{14.2}Sn_{2.7}$ structure. This direction corresponds to one of the six five-fold axes of the complex atomic cluster building the structure. The orientation of the cluster in the cubic cell along one of these particular axes is presented in figure 3(b.) In figure 3(a), all reflections can be indexed in the cubic lattice. The most intense reflections, with high hkl values, form a pattern consisting of a pseudo-decagonal ring around the central spot together with pentagonal motifs, in agreement with a local atomic structure built according to icosahedral symmetry. These zone axes are

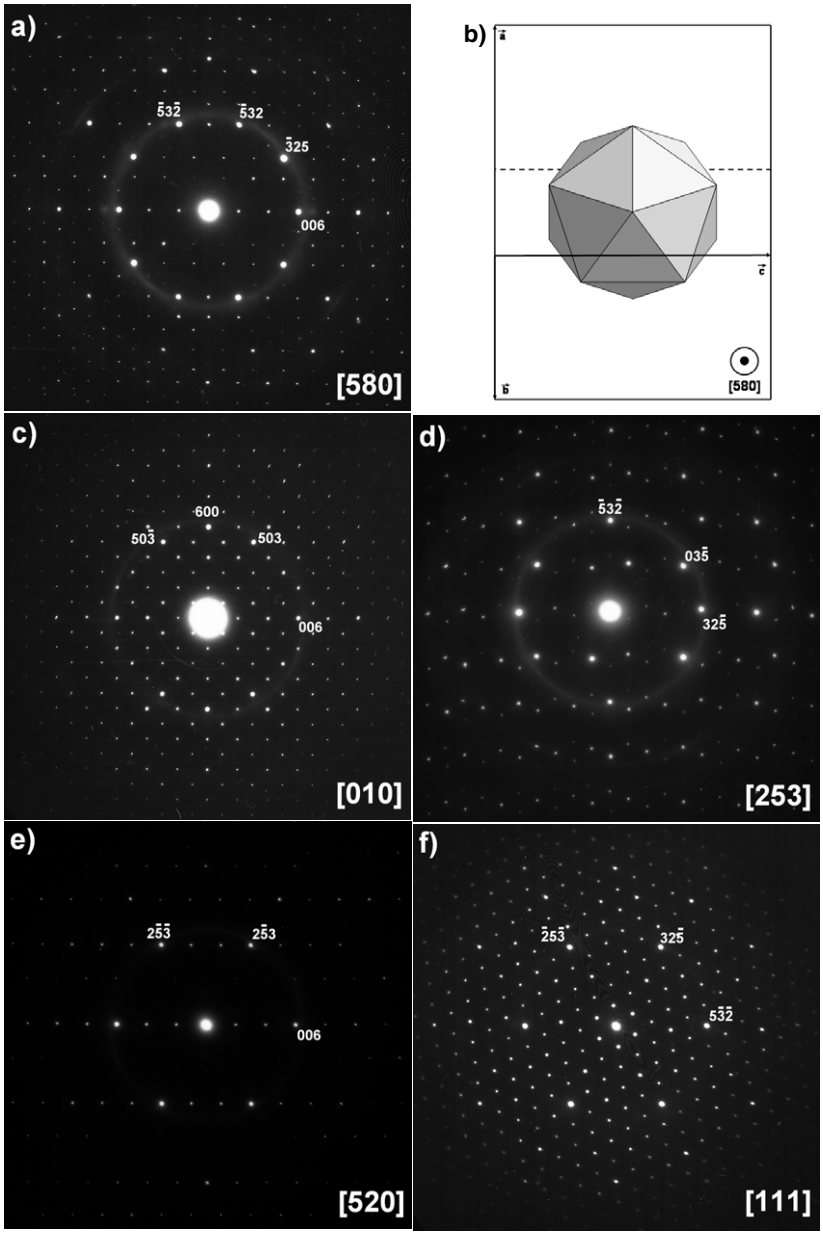

Figure 3. (a) EDP along the [580] zone axis of the bcc $Ce_{15}Au_{65}Sn_{20}$; (b) schematic of the cubic cell along the same direction, showing the orientation of the central atomic cluster; (c) EDP along the [010] zone axis; (d)–(f) the same along [253], [520] and [111], respectively.

called pseudo-five-fold (P5) axes. The remaining characteristic directions of the icosahedral symmetry, namely the two-fold and three-fold axes, are of two types each. The two kinds of pseudo-two-fold (P2) axes are the $\langle 010 \rangle$ and $\langle \tau^{-2} 1 \tau^{-1} \rangle$ (close to $\langle 253 \rangle$) directions, respectively, and are displayed in the EDPs in figures 3(c) and (d). The pseudo-three-fold (P3) axes are the $\langle 1 \tau^{-2} 0 \rangle$ (close to $\langle 520 \rangle$) and $\langle 111 \rangle$ directions and are displayed in the EDPs in figures 3(e) and (f), respectively. All these diffraction patterns are characteristic of an approximant structure and are similar to those calculated or observed in 1/1 cubic approximant crystals in Cd–Yb, Cd–Ca or Ag–In–Dy systems [13, 19].

The construction of the stereographic projection considering this indexing scheme is represented in figure 4 and is very similar to the one observed for the icosahedral phase [20]. It confirms that this phase is an approximant of the quasicrystalline structure.

In the same sample, a hexagonal structure (with $a \approx 1.32$ nm and $c \approx 0.95$ nm) was also identified by TEM, although it was not detected in the x-ray powder pattern. Figure 5 presents the EDPs of this structure along the [001] and [100] zone axes. A similar structure is also present in the Cd–Yb system [21], and in related binary systems as well [22]. This phase belongs to the $Ag_{51}Gd_{14}$ structure type (hP68, P6/m) and is linked to the icosahedral symmetry. Indeed, according to the structure determination of $Au_{51}RE_{14}$ by Bailey *et al* [23], nearly icosahedral environments can be found around specific sites in the unit cell. These local environments are outlined in the structure model presented in figure 6. Nevertheless,

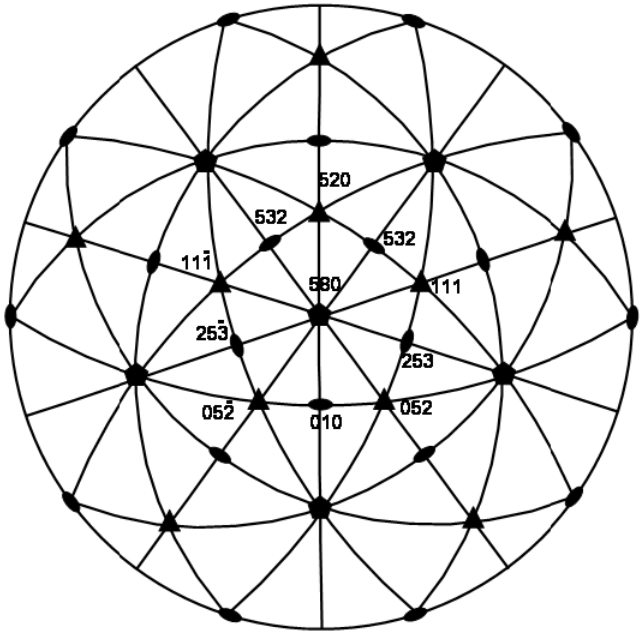

Figure 4. Stereographic projection showing the principal symmetry directions P5, P2 and P3 of the bcc $Ce_3Au_{14.2}Sn_{2.7}$ as seen along the pseudo-5-fold axis.

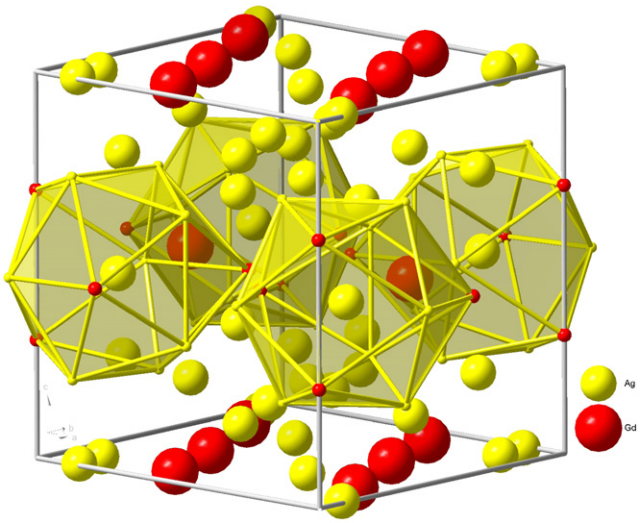

Figure 6. Icosahedral clusters in the hexagonal $Ag_{51}Gd_{14}$ structure type.

this structure is not considered as a close approximant of icosahedral quasicrystals [24].

3.3. Electronic structure by photoemission spectroscopy

The valence band spectrum of the $Ce_{15}Au_{65}Sn_{20}$ compound is shown in figure 7. Due to photo-ionization cross-section effects, the spectrum is dominated by the Au 5d levels at 4.5 and 6.6 eV below the Fermi level (E_F). Note that Ce atoms have one f electron, but 4f states cannot contribute to the He I spectra ($\hbar\omega = 21.2$ eV), even for pure Ce metal, due to their low photo-ionization cross section at this photon energy [25, 26]. Therefore the intensity plateau observed between the Au d band and E_F originates from Au, Sn and Ce sp states only. In the vicinity of the Fermi level, the spectral intensity exhibits a small maximum at ∼0.85 eV below E_F (figure 8(a)) and a subsequent decrease as E_F is approached. We believe that this feature is the signature of a pseudo-gap in the density of states produced by the scattering of sp electrons by Bragg planes, producing Van Hove singularities in the density of states (DOS). Similar features in the photoemission intensity measured in icosahedral (i-) i-ZnMgY, i-ZnMgHo and i-ZnMgEr quasicrystals were interpreted in the same way [27, 28]. As the valence bands of these quasicrystals are also determined by sp electrons in the vicinity of E_F, it was found that the near-Fermi-edge photoemission spectra could be well reproduced assuming a linear density of states $N_0(\varepsilon) = [b + a(\varepsilon - \varepsilon_F)]$ modulated by a pseudo-gap function $P(\varepsilon)$, i.e. $N(\varepsilon) = N_0(\varepsilon)[1+P(\varepsilon)]$. The pseudo-gap function can be calculated analytically within the nearly free electron approximation and a two-band model. The scattering by Bragg planes produces Van Hove singularities in $N(\varepsilon)$ at $\varepsilon = \hbar^2(1/2g)^2/2m$, where $(1/2g)$ defines Bragg planes nearly tangent with the Fermi sphere of radius k_F. The Fermi wavevector $k_F = (3\pi n)^{1/3}$ of our Ce–Au–Sn compound can be calculated assuming valences of +3, +1 and +4 for Ce,

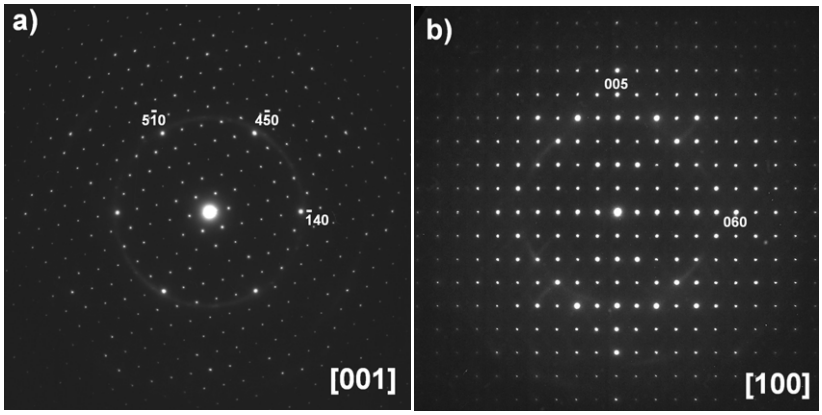

Figure 5. (a) EDP along the [001] zone axis of the hexagonal $Ag_{51}Gd_{14}$ structure type observed in the Ce–Au–Sn system; (b) the same along [100].

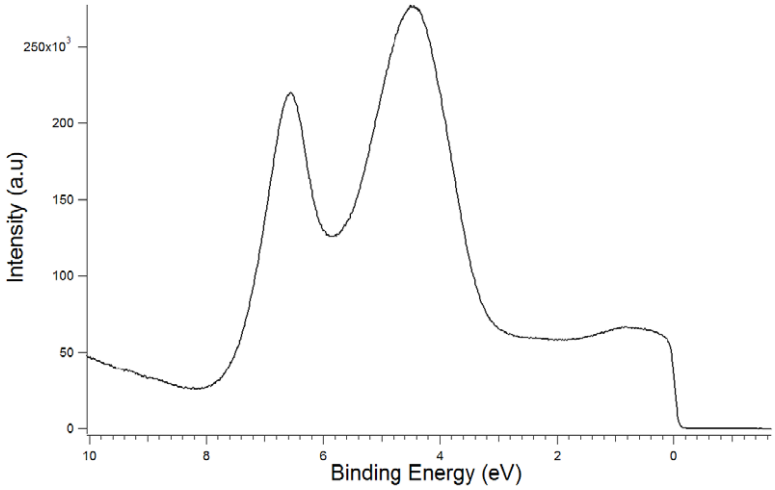

Figure 7. He I valence band spectrum of the $Ce_{15}Au_{65}Sn_{20}$ compound. The two main peaks originate from the Au d band.

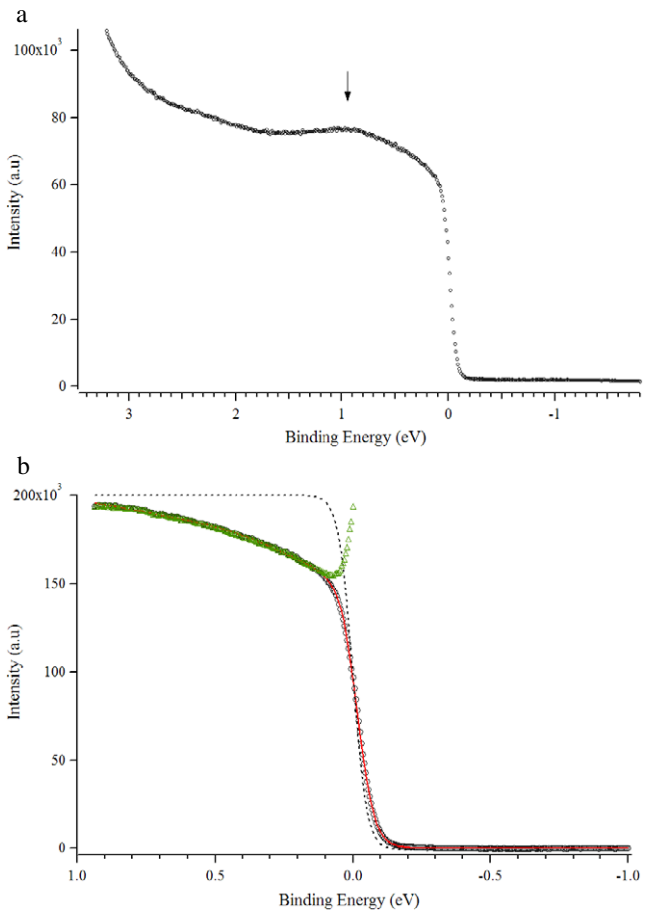

Figure 8. (a) The near-Fermi-edge spectra, showing a maximum intensity at 0.85 eV; (b) the measured spectral intensity (circles) can be fitted by the pseudo-gap function (red curve). The calculated Fermi function at 300 K (black dotted curve) is used to reconstruct the spectral function of the valence band near E_F (green curve).

Au and Sn, respectively, and a unit cell containing 161 atoms with an average valence of e/a $\sim$ 1.91. The valence for Ce atoms is consistent with magnetic susceptibility measurements, indicating a Curie–Weiss behaviour with an effective magnetic moment of 2.60 μ_B/Ce atom, which corresponds to Ce^{3+} [17]. This value of e/a leads to a value of $k_F = 1.37$ Å^{-1}, defining a Fermi surface nearly tangential to the effective Brillouin zone constructed from the (514) and (613) Bragg planes ($1/2g_{514} = 1.34$ Å^{-1}, $1/2g_{613} = 1.40$Å^{-1}). The interaction of the Fermi sphere with this nearly spherical Brillouin zone (96 facets) results in the formation of the pseudo-gap. Figure 8(b) shows the near-Fermi-edge spectra recorded at 300 K. The measured intensity can be expressed as the spectral function $S(E)$ multiplied by the Fermi function $f(E, T)$, to account for the reduced occupation probability for states near and above E_F, and convoluted by the instrumental function $G_{exp}(E)$:

$$I(E) = \int S(x) f(x, T) G_{exp}(x, E)\, dx.$$

We use the approximation first proposed by Mori *et al* [29] to model the spectral function and fit the near-Fermi-edge spectra:

$$S(E) = N(ax + b)\left(1 - \frac{C\Gamma_L^2}{x^2 + \Gamma_L^2}\right).$$

This assumes again a linear density of states modulated by a pseudo-gap function, which in this case is a Lorentzian function centred at E_F. The pseudo-gap is thus characterized by a half-width Γ_L and a depth C relative to the normal DOS. The result of the fit is shown by the red curve in figure 8(b) and, as can be seen, nicely reproduces the experimental data. Numerical values derived from the fit leads to a 20% reduction in the intensity at E_F compared to the normal DOS and a full-width at half maximum of 1.2 eV for the pseudo-gap.

To gain some insight into the spectral function above the Fermi level, we divide the measured intensity by the Fermi function at 300 K (black dotted curve). This procedure takes into account the fact that states above E_F can be populated according to the Fermi function at 300 K and thus can be probed by photoemission, at least in a narrow energy range above E_F [30, 31]. The result is shown as the green curve

in figure 8(b). Neglecting variation in the transition matrix elements, the spectral function is equivalent to the DOS and shows a minimum located slightly below E_F, at a binding energy of 0.07 eV.

These measurements demonstrate the formation of a shallow pseudo-gap in this alloy, in a way similar to what is observed in other quasicrystalline systems and related complex metallic alloys. The pseudo-gap appears to be located slightly below E_F and originates from Van Hove singularities produced by the interaction of the Fermi surface with the effective Brillouin zone constructed from the (514) and (613) Bragg planes.

4. Conclusion

A sample with nominal composition $Ce_{15}Au_{65}Sn_{20}$ was prepared by arc-melting and was investigated by x-ray diffraction and transmission electron microscopy. It crystallizes in the body-centred cubic system ($a = 1.5190$ nm) and the structure is refined in the centrosymmetric space group $Im\overline{3}$. As in the $Zn_{17}Sc_3$ 1/1 approximant, large atomic clusters with icosahedral symmetry are located at the node of the bcc unit cell and consist of three concentric shells. The Ce atoms only occupy positions forming an icosahedral shell within the cluster building blocks. Electron diffraction patterns characteristic of an approximant structure were observed by TEM and demonstrate similarities with the 1/1 cubic approximant crystals in the Zn–Sc and Cd–Yb systems. The valence band of the $Ce_{15}Au_{65}Sn_{20}$ cubic approximant has been measured by photoemission spectroscopy and shows an indication of a shallow pseudo-gap in the density of states, characteristic of quasicrystalline and related phases. By substituting Ce by other rare-earth (RE) elements, it is expected that many different RE–Au–Sn 1/1 approximants could be discovered, and this was confirmed recently by Tsai [32]. We also expect the discovery of new icosahedral phases in such systems by investigating nearby regions in the phase diagram.

Acknowledgments

We acknowledge the European Network of Excellence on Complex Metallic Alloys (CMA) contract NMP3-CT-2005-500145. We would also like to thank S Migot for her help in the preparation of the TEM samples and D Bonina for performing the energy dispersive x-ray analysis and B Malaman for providing cerium metal.

References

[1] Kaneko Y, Arichika Y and Ishimasa T 2001 *Phil. Mag. Lett.* **81** 777
[2] Palenzona A and Manfrinetti P 1997 *J. Alloys Compounds* **247** 195
[3] Andrusyak R I, Kotur B Ya and Zadovnik V E 1989 *Kristallografiya* **34** 996
[4] Ishimasa T, Kaneko Y and Kaneko H 2002 *J. Alloys Compounds* **342** 13
[5] Maezawa R, Kashimoto S and Ishimasa T 2004 *Phil. Mag. Lett.* **84** 215
[6] Ishimasa T, Kaneko Y and Kaneko H 2004 *J. Non-Cryst. Solids* **334/335** 1
[7] Ishii Y and Fujiwara T 2004 *J. Non-Cryst. Solids* **334/335** 336
[8] Ishii Y and Fujiwara T 2001 *Phys. Rev. Lett.* **87** 206408
[9] Ishii Y and Fujiwara T 2002 *J. Non-Cryst. Solids* **312–314** 494
[10] Gomez C P and Lidin S 2003 *Phys. Rev.* B **68** 024203
[11] Takakura H, Gomez C P, Yamamoto A, de Boissieu M and Tsai A-P 2007 *Nature* **6** 58
[12] Guo J Q, Abe E and Tsai A-P 2002 *Phil. Mag. Lett.* **82** 349
[13] Ruan J F, Kuo K H, Guo J Q and Tsai A-P 2004 *J. Alloys Compounds* **370** L23
[14] Iwano S, Nishimoto K, Tamura R and Takeuchi S 2006 *Phil. Mag.* **86** 435
[15] Singh A, Guo J Q and Tsai A-P 2007 *Mater. Sci. Eng.* A **449–451** 991
[16] Tsai A-P 2004 *J. Non-Cryst. Solids* **334/335** 317
[17] Boulet P, Mazzone D, Noël H, Rogl P and Ferro R 2001 *J. Alloys Compounds* **317/318** 350
[18] Rodriguez-Carvajal J 1993 *Physica* B **192** 55
[19] Takakura H, Guo J and Tsai A P 2001 *Phil. Mag. Lett.* **81** 411
[20] Cahn J W, Shechtman D and Gratias D 1986 *J. Mater. Res.* **1** 13
[21] Palenzona A 1971 *J. Less-Common Met.* **25** 367
[22] McMasters O D, Gschneider K A, Bruzzone G and Palenzona A 1971 *J. Less-Common Met.* **25** 135
[23] Bailey D M and Kline G R 1971 *Acta Crystallogr.* B **27** 650
[24] Wu D, Ugurlu O, Chumbley L S, Kramer M J and Lograsso T A 2005 *Phil. Mag.* **86** 381
[25] Hüfner S 2003 *Photoelectron Spectroscopy: Principles and Applications* (Berlin: Springer) p 160
[26] Garnier M, Purdie D, Hengsberger M, Breuer K and Baer Y 1999 *Physica* B **259–261** 1095
[27] Suchodolskis A, Assmus W, Giovanelli L, Karlsson U O, Karpus V, Le Lay G, Sterzel R and Uhrig E 2003 *Phys. Rev.* B **68** 054207
[28] Suchodolskis A, Assmus W, Giovanelli L, Karlsson U O, Karpus V, Le Lay G and Uhrig E 2004 *J. Phys.: Condens. Matter* **16** 9137
[29] Mori M, Matsuo S, Ishimasa T, Matsuura T, Kamiya K, Inokuchi H and Matsukawa T 1991 *J. Phys.: Condens. Matter* **3** 767
[30] Neuhold G, Barman S R, Horn K, Theis W, Ebert P and Urban K 1998 *Phys. Rev.* B **58** 734
[31] Hüfner S 2003 *Photoelectron Spectroscopy: Principles and Applications* (Berlin: Springer) p 162
[32] Tsai A P Oral presentation given at the *Conf. on Quasicrystals: The Silver Jubilee (Tel-Aviv, October 2007)*